

# Structured Image Classification from Conditional Random Field with Deep Class Embedding

Ernan Goldman<sup>1,2</sup> and Jacob Goldberger<sup>1</sup>

<sup>1</sup>Engineering Faculty, Bar-Ilan University, 52900 Ramat Gan, Israel

<sup>2</sup>Trax Image Recognition

## Abstract

This paper presents a novel deep learning architecture to classify structured objects in datasets with a large number of visually similar categories. Our model extends the CRF objective function to a nonlinear form, by factorizing the pairwise potential matrix, to learn neighboring-class embedding. The embedding and the classifier are jointly trained to optimize this highly nonlinear CRF objective function. The non-linear model is trained on object-level samples, which is much faster and more accurate than the standard sequence-level training of the linear model. This model overcomes the difficulties of existing CRF methods to learn the contextual relationships thoroughly when there is a large number of classes and the data is sparse. The performance of the proposed method is illustrated on a huge dataset that contains images of retail-store product displays, taken in varying settings and viewpoints, and shows significantly improved results compared to linear CRF modeling and sequence-level training.

## 1. Introduction

Object recognition is one of the fundamental problems in computer vision. It involves finding and identifying objects in images, and plays an important role in many real-world applications such as advanced driver assistance systems, military target detection, diagnosis with medical images, video surveillance, and identity recognition.

Over the past few years deep convolutional neural networks (CNN) have led to a remarkable progress in image classification [18, 12], and resulted in reliable appearance-based detectors e.g. [25, 21, 10, 24]. Fine-grained object recognition aims to identify subcategory object classes, which includes finding subtle difference among visually similar subcategories. Recent studies achieved good performance on fine-grained tasks [20, 33]. However, the problem



Figure 1. Spot the difference: Examples of classes with similar appearance. Each product in each grouping in this image belongs to a different category.

remains extremely difficult when the dataset categories are nearly identical in terms of their visual appearance. In this case, object categories are often virtually indistinguishable, since the discriminative features may be masked by inadequate observation or visual artifacts.

This study addresses the problem of classifying a sequence of objects based on their visual appearance and their relative locations. Our dataset contains photos of retail-store product displays, taken in varying settings and viewpoints. The objects are the products at the front of the shelves. The dataset is exclusively characterized by having a distinct geometric object structure, a large number of classes, and very subtle visual differences between groups of classes. The unique challenges in this task involve handling the large number of possible classes, and the fact that the classes are not clearly distinctive by their appearance but rather by their context. For example, products with identical appearance but with different container volumes are considered different classes (see examples at Fig. 1, 2).

Because the object local appearance may not suffice for accurate categorization, additional information needs to be considered. In real world images, contextual data provides useful information about spatial and semantic relationships between objects. Modeling a joint visual-contextual classifier is nontrivial in that some contextual cues are very informative, whereas others are irrelevant, or even misleading. Most deep learning detectors classify each detected object individually without taking the contextual information into account.

Many techniques have used context to improve performance for image understanding tasks [30, 7, 9]. Graphical models have been widely applied to visual and auditory analysis tasks, by jointly modeling local features, and contextual relations. Some of the tasks addressed by these models include image segmentation and object recognition [11, 32, 34, 28], as well as speech [31], music [17], text [1, 4] and video analysis [14].

Few studies have applied deep learning features or detection results to context models: Chu and Cai [6] evaluated the performance of a joint CRF model on Faster R-CNN [25] detection results. Their CRF model takes the detection unary potentials from their network prediction results, and the inter-detection pairwise potentials from an a-priori statistical summary of spatial class relations. The trade-off between pairwise and unary potentials is calibrated by a fixed parameter. Korzeniowski and Widmer [17] introduced a two-stage learning model for musical chord recognition: one networks learns a single-frame representation, and the other learns the frame and inter-frame potentials of a linear-chain CRF model, using the frame-representations as the CRF input. These two CRF models use pairwise potentials to represent object-pair interaction. They allocate a different parameter for each class pair. This approach, which ignores class similarities, can work in small sets of distinct classes. However, it is not suitable for a large class-set that contains visually similar classes.

We present a novel method to classify structured objects in datasets with a large number of categories: Our model extends the CRF objective function to a nonlinear form, by factorizing the pairwise potential matrix. The generated matrix factors learn the neighboring-class embedding, and are trained jointly with local visual representations to optimize a nonlinear score function of a linear-chain CRF. Sequence-level training is optimal for the standard linear CRF model. In the model proposed in this study the likelihood function is not concave and therefore the optimization is more complicated than linear CRF. To find the model parameters we apply object-level training which is much faster than the standard sequence-level training of the linear model. We also show that this training strategy yields improved results on a large dataset. The rest of the paper is organized as follows. In the next section we describe a

CRF model with class embedding formulation and present the learning and inference algorithms. Section 3 contains a detailed data description and comparative experimental results.

## 2. CRF With Class Embedding

### 2.1. Model Formulation

Linear-chain Conditional Random Field (CRF) [19] is a type of discriminative undirected probabilistic graphical model, whose conditional distribution  $p(y|x)$  obeys a conditional Markov property. The joint probability distribution of a linear-chain CRF is:

$$p(\mathbf{y}|\mathbf{x}) = \frac{1}{Z} \prod_{t=1}^n \varphi(y_t, x_t, y_{t-1}) \quad (1)$$

where  $\mathbf{x} = [x_1, x_2 \dots, x_n]$  the sequence of observation feature vectors,  $\mathbf{y} = [y_1, y_2 \dots, y_n]$  the corresponding sequence of the target labels,  $\varphi$  the model potential function, and  $Z$  the global probability normalization factor over all possible sequence label-assignments of length  $n$ . For simplicity we assume  $y_0 = 0$ . Assume that the potential function is defined as:

$$\varphi(y_t, x_t, y_{t-1}) = \exp(y_{t-1}^\top P y_t + x_t^\top U y_t + y_t^\top b) \quad (2)$$

where matrix  $P$  the pairwise potentials matrix,  $U$  the unary potentials, and vector  $b$  the label bias, are all model parameters, and we use a one-hot encoding for the labels. The score function is log-linear and concave.

Our dataset contains spatially ordered sequences of image detections. We can train a local CNN to classify individual objects, and then interpret the hidden layer activations as a non-linear representation of the input image [3]. Similarly to the concept of transfer-learning, we can now discard the CNN softmax layer, and use the convolutional layers to compute the feature-vectors of the input images. For image-detection  $x_t$  we define the feature vector  $h_t = h(x_t)$  as the activations of the last fully-connected hidden layer, and use it as the CRF input observation feature vector:

$$\varphi(y_t, h_t, y_{t-1}) = \exp(y_{t-1}^\top P y_t + h_t^\top U y_t + y_t^\top b) \quad (3)$$

Combining neural networks with CRFs gives a fully differentiable model that can be learned jointly, as shown e.g. in [23, 8]. For the task at hand, however, we found it advantageous to train both parts separately, both in terms of convergence time and performance. The score function (3) is still concave, but its input is computed from a non-concave source, a deep CNN. The rationale for using deep representation for the input images is clear: as introduced by Krizhevsky *et al.* [18], the immense complexity of the visual object recognition task requires a model with a very

large learning capacity. In our exceptional case, deep representations should be considered for the contextual relations as well.

CRF was originally applied to language processing tasks such as Part of Speech (POS) tagging and Named Entity Recognition (NER) [19]. In most applications of CRF to either language or image understanding, there are no more than a few dozen different classes. In our dataset, we have hundreds of classes. The pairwise transition between two classes has nearly a million possible states, whereas the CRF function (3) has a log-linear form, and contains a single parameter per transition ordered-pair. In order to properly learn and generalize the massive variety of possible neighboring patterns, we enforce a structure on the pairwise potential matrix: the goal is to learn neighboring-class embedding in a feature vector space. For this purpose, we define a low-dimensional decomposition of the pairwise potential matrix  $P$  as the product of the left-side neighbor embedding matrix  $R$  and the class embedding matrix  $Q$ :

$$P = R^\top Q \quad (4)$$

The columns of  $Q$  are low-dimensional embeddings of the target classes, and the columns of  $R$  are embeddings of the classes of the left-side object. Assigning the matrix factorization (4) to the CRF potential function (3) we get:

$$\varphi(y_t, h_t, y_{t-1}) = \exp(y_{t-1}^\top R^\top Q y_t + h_t^\top U y_t + y_t^\top b). \quad (5)$$

The CRF score function is no longer log-linear or concave, but modern deep learning techniques have been shown to yield good results for non-convex optimization tasks [5]. This simply means that we need to apply the deep learning approach not only for the input image representations, but also for the neighboring transition parameters.

We originally considered other variants of the class embedding concept, including the same embedding for the class and its neighbor by setting the decomposition of the pairwise potential  $P$  to satisfy  $R = Q$ . We also applied the class embedding on the unary potential  $U$ . All these variants, however, performed less well than the baseline linear CRF. The main information source, in addition to the object recognition CNN, is the object pairwise statistics.

## 2.2. Training

The CRF model [19] can be trained in a supervised manner by maximizing the log-likelihood of all sequences in the training dataset:

$$\mathcal{L}(R, Q, U, b) = \sum_{i=1}^S \log p(\mathbf{y}_i | h(\mathbf{x}_i)) \quad (6)$$

where the vector  $\mathbf{y}_i$  contains the ground-truth labels of the  $i^{\text{th}}$  sequence,  $h(\mathbf{x}_i)$  contains the corresponding object feature vectors of the sequence of observations and  $i$  goes over

the sequences in the training data. This training process takes a great deal of time, because it needs to compute the global normalization factor  $Z$  for each sequence. The normalization factor can be calculated by the forward algorithm, but is still relatively slow for a large number of classes.

Linear-chain CRFs were originally introduced as an improvement on the maximum entropy Markov model (MEMM) [22], which is essentially a Markov model in which the transition distributions are given by a logistic regression model. The main difference between CRFs and MEMMs is that a MEMM uses per-state exponential models for the conditional probabilities of next-states given the current-state, whereas the CRF has a single exponential model for the joint probability of the entire sequence of labels given the observation-sequence. CRF and MEMM can be written using the same set of parameters. The MEMM directed graphical modeling in our case is:

$$p(\mathbf{y} | h(\mathbf{x})) = \prod_t p(y_t | h_t, y_{t-1}) \quad (7)$$

where

$$p(y_t | h_t, y_{t-1}) = \frac{1}{Z(t)} \exp(y_{t-1}^\top R^\top Q y_t + h_t^\top U y_t + y_t^\top b) \quad (8)$$

One major advantage of MEMMs over CRFs (and HMMs) is that training can be considerably more efficient. In CRFs, some version of the forward-backward algorithm needs to be used as an inner loop in training. However, in MEMMs, the parameters of the maximum-entropy distributions used for the transition probabilities can be estimated for each transition distribution separately. MEMM, however, is known to suffer from the label bias problem [19, 16] which may lead to a drop in performance in some applications. Intuitively, we want the model to be able to revise an earlier decision made during search when later evidence becomes available that rules out the earlier decision as incorrect. The label bias problem means that when inference is computed locally, normalized models often have a very weak ability to revise earlier decisions. Note that the label bias is an inference step problem of the MEMM model. In MEMM *training*, however, each object is treated separately; thus label bias does not apply to training.

Here we apply the MEMM training procedure to learn the parameter set of the CRF model. We use the MEMM framework solely for learning the CRF parameters, whereas the test time inference uses a global normalization of CRF modeling and thus avoids the label bias problem. We denote this procedure as CRF *object-level training* as opposed to standard CRF *sequence-level training*. The standard sequence-based CRF training finds the global maximum of the CRF likelihood, which is a concave function. In our modeling, which is based on class embedding, the objective

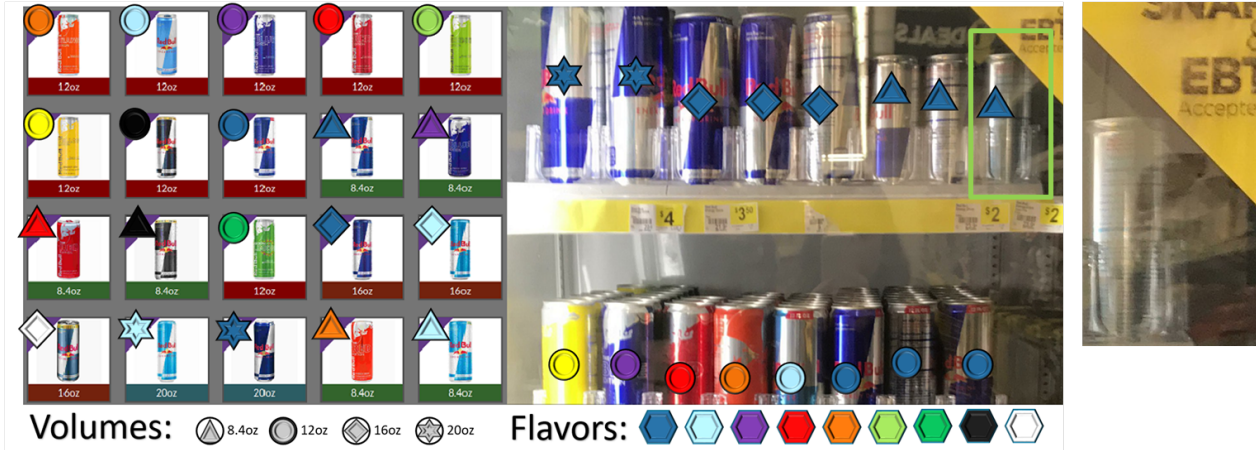


Figure 2. Scene example with the relevant classes presented on the left. For some of the products in this scene, classification based on local appearance alone would be extremely difficult even for expert humans. The object on the top right, for instance, is partially occluded, and visually distorted by reflections, illuminations, and focus. Additionally, it is facing backwards, making its flavor undetermined. When viewed separately, the volume cannot be determined either. Shelf-level classification exploits the information extracted from the other items and their spatial relations, including a-priori knowledge of structure statistics, to jointly determine the shelf classes.

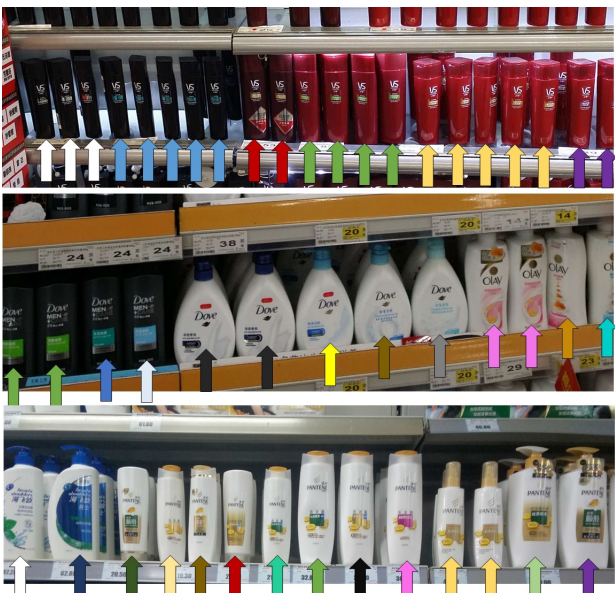


Figure 3. Examples of display shelves. Each arrow color represents a different class. Some typical patterns are evident.

function is not concave and thus can have many maxima points. Hence, there is no guarantee that a sequence-level training converges to the global maximum point, and there is no theoretical reason to prefer sequence training over MEMM-like object training which is much faster. Since the images capture arbitrary subsections of the shelf displays, the visual appearances of object sequence in a shelf vary unpredictably in terms of their relative positions and

occasional unnoticed or absent elements. Nevertheless, the co-occurrence data statistics remains stable in most cases, which justifies the stationarity and Markovity assumptions of our model. We argue that breaking the samples from sequences into adjacent pairs does not eliminate significant contextual information. Rather, it may enrich the training dataset, improve the stochastic nature of the SGD optimization process, and help prevent overfitting since there are many more object samples than sequence samples, and the mini-batches are composed of adjacent pairs of objects taken from random training samples. In contrast, restricting the mini-batches to contain full sequences, would decrease the model’s freedom to discover better solutions for the objective of pairwise transition parameters. In fact, as we empirically show in the next section, object-level training yields better results than sequence-level training.

We train by maximizing the likelihood function, which is the conditional probability of the current-object class, given the class of the left-side neighbor object. The objective function is now defined as:

$$\mathcal{L} = \sum_i \sum_t \log p(y_{i,t} | h_{i,t}, y_{i,t-1}) \quad (9)$$

where  $i$  goes over the sequences and  $t$  goes over the objects in the sequence,  $h_{i,t}$  is the object CNN-based representation and  $y_{i,t}$  is the true class label. In this case, the global normalization factor is not required, and the training process is much faster. During training, the label of the left-side object is known. At test time, the label sequence is not known and we need to apply a forward-backward procedure to compute the label probabilities.

### 2.3. Inference

At test time, sequence-level classification is applied to the linear-chain CRF. Dynamic programming algorithms may be used for efficient and exact inference as follows: the Viterbi algorithm finds the most probable sequence label assignment, and the Forward-Backward algorithm extracts the marginal probability of each item, by summation over all possible assignments [29]. Note that although the training was done with object-level samples, and we assumed that the predecessor label is known, at test time we apply the global normalization over all possible object sequences.

### 2.4. Implementation Details

We first train a Krizhevsky CNN [18] to compute the hidden representation vector  $\mathbf{h}_{s \times 1}$  for each image-patch. In our implementation we the hidden layer size was  $s = 2048$ . As a preprocessing step, we go over the training dataset to calculate the mean and standard deviation of each feature of the hidden representation vector:  $\mu_{s \times 1}, \sigma_{s \times 1}$ .

The number of classes in our dataset is  $m = 972$ , and the class embedding dimensionality we use is  $d = 32$ . The CRF training is used to find a class embedding matrix  $Q_{d \times m}$ , a neighbor embedding matrix  $R_{d \times m}$ , a unary potential matrix  $U_{s \times m}$  and a bias vector  $\mathbf{b}_{m \times 1}$ . We train the network in a supervised manner as described in subsection 2.2, using SGD with mini-batches of size 128, and maximizing the log-likelihood function (9) with an  $l_2$  regularization factor  $\lambda = 5 \cdot 10^{-4}$  for all network parameters. The training samples in each mini-batch are object-pairs selected randomly from the benchmark. Each sample is a horizontally adjacent pair of left-label  $\mathbf{y}_{m \times 1}$  in a one-hot encoding, and right image-patch representation  $\mathbf{h}_{s \times 1}$ . If the object has no left neighbor,  $\mathbf{y}$  is assigned to the zero vector, so the pairwise related parameters are not affected. The neighbor embedding matrix  $R_{d \times m}$  is learned by a fully connected layer which receives the left-label one-hot vector  $\mathbf{y}_{t-1}$  and returns the corresponding left-embedding vector  $\mathbf{r}_{\mathbf{y}_{t-1}}$ . The fully-connected embedding layer is trained with batch-normalization [15]. A normalization is also applied on the right image-patch representation  $\mathbf{h}_t$  by subtracting the pre-calculated  $\mu$  and dividing by the pre-calculated  $\sigma$ . The standardized vectors are concatenated as  $\mathbf{f}_t = (\mathbf{r}_{\mathbf{y}_{t-1}} \quad \mathbf{h}_t)$ , which is the input of the softmax layer, composed of the weights  $(Q^T \quad U^T)^T$ , and bias  $\mathbf{b}$ . The feature vector standardization is important to avoid inherent bias between the local-visual information. At test-time, we compute the non-linear representation vector  $\mathbf{h}$  of each object in the sequence, normalize each of its features by the pre-calculated  $\mu$  and  $\sigma$ , and classify the objects as described in subsection 2.3.

**Training data:** Feature sequences  $\mathbf{x}_1, \dots, \mathbf{x}_n$  with corresponding label sequences  $\mathbf{y}_1, \dots, \mathbf{y}_n$ .

**Training algorithm:**

- Train a CNN to maximize the likelihood:

$$\mathcal{L}_{\text{cnn}} = \sum_i \sum_t \log p(y_{i,t} | x_{i,t})$$

- Train a CRF to maximize the object-level score:

$$\mathcal{L}(R, Q, U, b) = \sum_i \sum_t \log p(y_{i,t} | h_{i,t}, y_{i,t-1})$$

$$\text{s.t. } p(y_{i,t} | h_{i,t}, y_{i,t-1}) =$$

$$\frac{1}{Z_{i,t}} \exp(y_{i,t-1}^T R^T Q y_{i,t} + h_{i,t}^T U y_{i,t} + y_{i,t}^T b)$$

and  $h_{i,t}$  is the CNN-based representation of  $x_{i,t}$ .

**Inference Algorithm:** Given an object sequence  $\mathbf{x}$ :

- Apply the CNN to obtain a non-linear representation  $\mathbf{h} = \mathbf{h}(\mathbf{x})$ .
- Apply the forward-backward (or Viterbi) algorithm on the CRF:

$$p(\mathbf{y} | \mathbf{x}) = \frac{1}{Z} \exp\left(\sum_t y_{t-1}^T R^T Q y_t + h_t^T U y_t + y_t^T b\right)$$

to find the labels of the object sequence.

Table 1. CRF with deep class embedding algorithm.

## 3. Experiments

### 3.1. The Dataset

Our dataset contains photos of retail-store displays, taken in supermarkets and grocery-stores. The images capture arbitrary subsections of the displays, in varying settings and viewpoints. The objects are the inventory items positioned at the front of the displays, and the classes are their stock-keeping-unit (SKU) unique identifiers. Each object is annotated by its class label and bounding-box coordinates. The objects in each image are grouped into *shelves* - sequences of horizontal layouts, sorted from left to right.

The benchmark contains 24,024 images, 76,081 sequences, and 460,121 objects, each labeled as one of 972 different classes. Sequence lengths can vary from 2 to 32, and are typically between 4-12. We split the dataset into 80% training and 20% testing.

Many groups of classes belong to the same archetype, and only differ in terms of minor details such as volume,

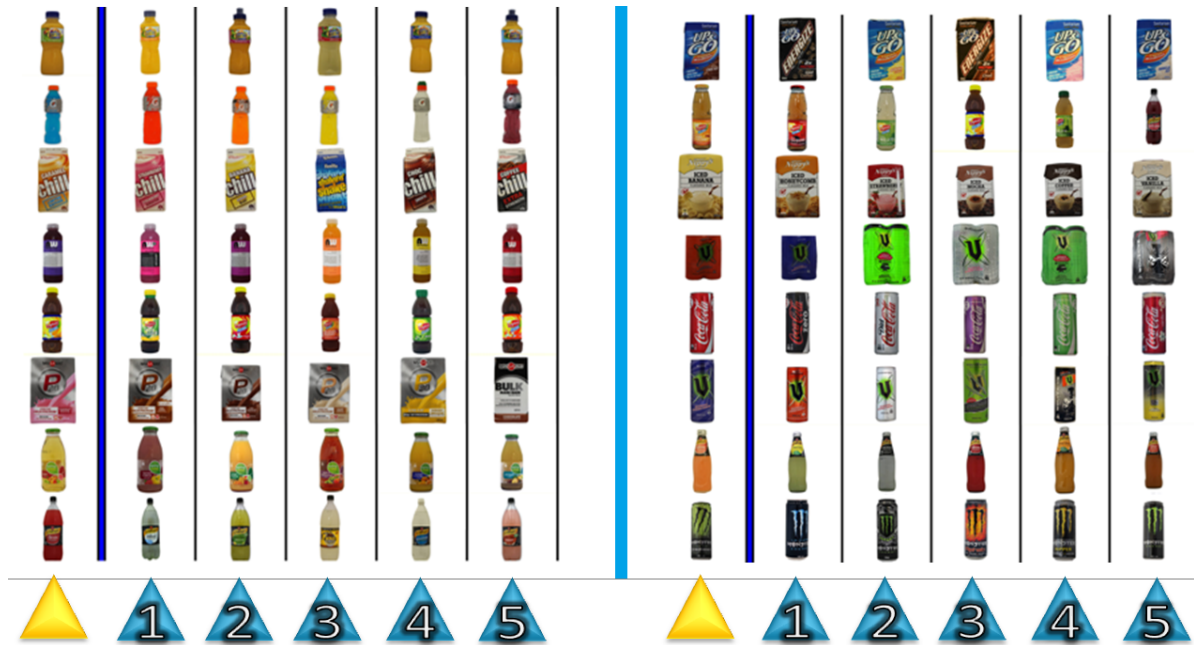


Figure 4. Class similarity examples. For each class we show five nearest neighbors based on cosine distance computed on the class embeddings.

flavor, nutrient-content etc. They often share similar visual features, which makes appearance-based classification very difficult (Fig. 2). On the other hand, the object layout behavior is very coherent: it is dictated by the supplier *planograms* (specified product layouts) and extracted from the image *realograms* (observed product layouts). Although realograms are non-deterministic by nature, consistent semantic patterns are frequently spotted. Class transition behavior may be discovered, revealing tendencies of pairs to appear as left-to-right neighbors, and individual classes to appear multiple times successively (Fig. 3). The unique challenges we face in our task are derived from the large number of visually similar classes, which co-occur in distinct structures in large-scale images.

### 3.2. Comparisons with Other Methods

In order to validate the performance of the proposed method we implemented several alternative methods. All the methods are based on the same context-less CNN local information. They differ in the way they learn the object context information from the training dataset and the way they integrate the context model with the local CNN soft-decision. Below is a list of the context models we implemented.

**Unary:** The baseline comparison model is the original CNN without any context information.

**Pairwise Statistics:** Following the work of [6], we created a CRF model with unary potentials taken from the

CNN classifier prediction results, and the pairwise potentials are pairwise statistic  $P_{ij} = p(j|i) = p(y_t = j | y_{t-1} = i)$  that are estimated from the training dataset. In other words, the context information is modeled by a stationary first-order Markov chain. No additional NN training is applied. The only single parameter we need to set is the relative weight of the unary and pairwise potentials. This weight, which adjusts the tradeoff between the local appearance and the contextual information, was selected via cross validation.

**Mixture of CRFs:** Still relying on the pairwise statistics summary model, we can also model global context information; for instance, the fact that all the objects in the sequence have the same label. We clustered the *sequences* into a mixture of  $k$  Markov models, using the Expectation-Maximization (EM) algorithm. The training sequences are eventually split into  $k$  different groups, and pairwise statistics are separably calculated for each one of them. At test time, the most probable Markov model is selected for each sequence, and the corresponding pairwise statistics CRF model is used. The mixture of  $k$  Markov models method was examined with  $k$  values ranging from 2 to 16. It revealed chain groupings to some extent, but did not lead to a significant improvement in the overall classification performance compared to the baseline CRF model of  $k = 1$ .

We also tried an alternative (or complementary) clustering approach, in which we grouped the *classes* into clusters that maximize the mutual information between consec-

Architecture	Regularization	Training Sample	Error %
Unary (no context)	l2	Object	15
BLSTM	l2	Object	15
Pairwise statistics CRF [6]	n/a	n/a	15
Mixture of CRFs	n/a	n/a	15
Linear CRF [17]	l1	Sequence	20
Linear CRF	l1	Object	20
Linear CRF	l2	Sequence	14.5
Linear CRF	l2	Object	14
Non-linear CRF with class embedding	l2	Sequence	13
Non-linear CRF with class embedding	l2	Object	11
Deeper Embedding	l2	Object	11

Table 2. Comparison of the object-level error rate between the different methods. Testing benchmark contains 90592 objects.

Architecture	Regularization	Training Sample	Recall %	Precision %
Unary	l2	Object	79	91
BLSTM	l2	Object	79	91
Pairwise statistics CRF	n/a	n/a	83	91
Linear CRF	l2	Sequence	81	91
Linear CRF	l2	Object	81	91
Non-linear CRF with class embedding	l2	Sequence	84	91
Non-linear CRF with class embedding	l2	Object	87	91

Table 3. Comparison of recall % when score acceptance threshold is calibrated to receive 91% precision.

tively visited groups [2]. The pairwise potential was then defined by pairwise statistics of the class clusters. Distinct clusters of classes were identified, but we did not manage to harness this information for the task of non-hierarchic class identification.

**Linear first-order CRF:** This method learns a linear CRF (3). We implemented both sequence-level and object-level training and we tried both  $l_1$  and  $l_2$  regularizations.

**Non-linear CRF with class embedding:** This is the main model described in this study, where the CRF is enhanced into a much richer, but non-convex model by extending the pairwise weight matrix as defined in Eq. (5). We implemented both sequence-level and object-level training procedures.

**Deeper Embedding:** We tried increasing the model’s non-linearity by adding another fully connected layer and nonlinear ReLU between the one-hot vector input and the fully connected embedding layer. It did not, however, improve performance, and turned out to be redundant.

**Recurrent Layers:** Another modeling option for a sequence estimation is Bi-Directional Recurrent Neural Network [26] with LSTM [13] as memory block (BLSTM). In that approach we compute the posterior distribution of label of the current object based on all the visual information provided by the CNN:

$$p(y_t|\mathbf{x}) = p(y_t|x_1, \dots, x_n) \quad (10)$$

In our case, however, the visual features over the sequence are much less informative than the label relations between neighboring objects, which are not captured here, and this approach did not yield any significant improvement over the original unary CNN.

### 3.3. Results

Table 2 describes the results in terms of model error rate, and portrays the incremental improvement in accuracy over model variations. In our model we used  $l_2$  regularization. We tried adding  $l_1$  regularization, but it did not work well for our data, probably because our input feature vector does not fit a sparse model. Table 2 reveals that the non-linear method that is based on class embedding showed better results than the linear model. We can also see that in the non-linear case object-level training yielded better results than sequence-level training. The best results are obtained for the non-linear model with object-level training. Table 3 refers to what was defined as our original objective: maximize recall while preserving at least 91% precision. It is interesting to note that our model, involving both object-level training and nonlinear CRF, is the only one that led to significant improvement over the pairwise statistical-summary model of [6] for this objective. It is worth pointing out that our benchmark is considerably large, which means that we correctly identified 7,200 more objects than the unary model, and 3,600 more objects than the pairwise-statistics model.

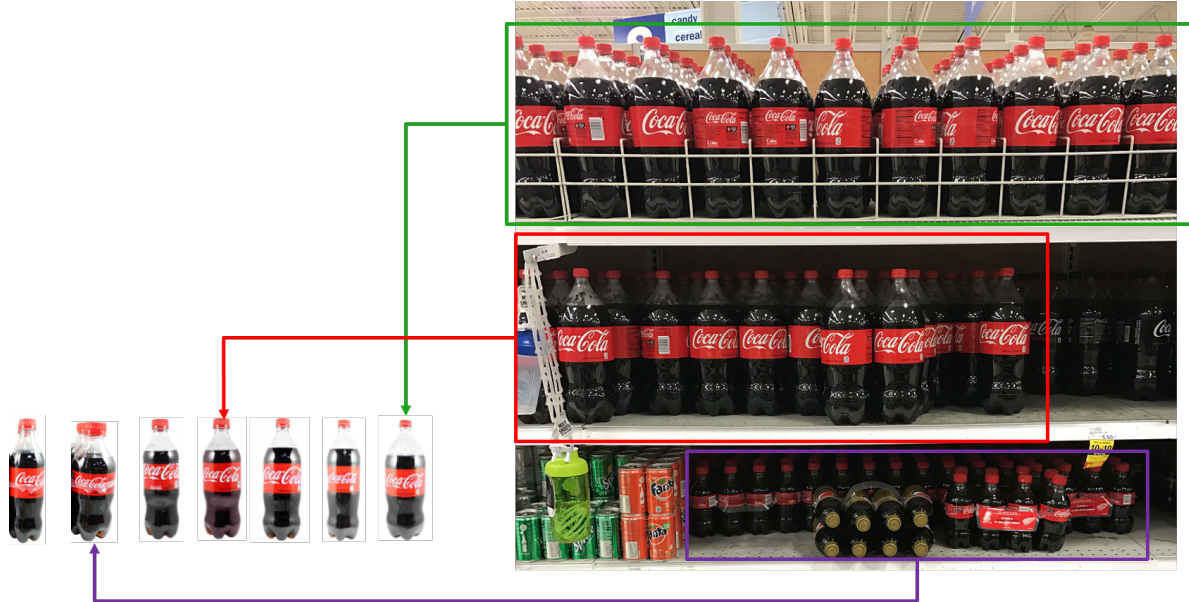


Figure 5. Example of a case where shelf-level classifications are not sufficient, and additional spatial relations need to be included in the model.

As a byproduct of the classification model we also obtain a low-dimensional embedding of the different classes. Each column of the neighbor embedding matrix  $R$  is vector representation of the corresponding class. A common similarity metric is the cosine of the angle between the vectors. We can measure the distance between classes by the cosine of their vector representation. Fig. 4 shows several examples of an object class and its most similar classes. We can see that this similarity does not reflect visual appearance similarity, e.g. in the second example the similar classes have very different colors. This situation was extensively studied for the linguistic problem of word embedding. The goal of word embedding algorithms is to represent similar words by similar vectors. It is often useful to distinguish two kinds of similarity or association between words [27]. Two words have first-order co-occurrence if they are typically nearby each other (e.g. write is a first-order associate of book or poem). Two words have second-order co-occurrence if they have similar neighbors (e.g. write is a second-order associate of words like said or remarked). Second-order word similarity is thus expected to capture a semantic meaning and measure the extent to which the two classes are replaceable based on their tendencies to appear in similar contexts. In Fig. 4 we show that object class embedding captures second-order information. Proximity here corresponds to the mutual tendency to have similar neighbors. We can see in Fig. 4 that similar classes, although look visually different, represent products of similar container-types, volumes and brands.

## 4. Conclusion

We introduced a novel technique to learn deep contextual and visual features for fine-grained structured prediction of object categories, and tested it on a dataset that contains spatial sequences of objects, and a large number of visually similar classes.

Our model clearly outperforms all the other tested models. This architecture appears to be the most straightforward generalization of a context-less classifier to be context-dependent when both the input and the context data require a large learning capacity: the network learns deep feature vectors for neighboring classes, analogously to the learned deep input representations. The Markovity and stationarity assumptions make it sufficient to train with individual objects as samples to enrich the training data diversity, allow for a simple embedding batch normalization, and boost the non-convex optimization process.

Shelf-level classification may not be sufficient in situation such as the one depicted in Fig. 5, where it may help identify a few probable shelf-classification possibilities, but no clear decision on the best one. This can be resolved by defining additional spatial-relationships in the graph, such as top-bottom edges, and learning their embedding. A scene-level classification may be inferred using a belief-propagation method. Efficient exact inference can be performed on a spanning-tree of the graph. Additional improvement may be achieved by integrating the bounding-box dimensions as part of the model input, or adding recurrent layers to model sequence to sequence relations.

## References

- [1] M. Abramson. Sequence classification with neural conditional random fields. In *Machine Learning and Applications (ICMLA)*, pages 799–804. IEEE, 2015. 2
- [2] A. Alush, A. Friedman, and J. Goldberger. Pairwise clustering based on the mutual-information criterion. *Neurocomputing*, 182:284–293, 2016. 7
- [3] Y. Bengio, A. Courville, and P. Vincent. Representation learning: A review and new perspectives. *IEEE Transactions on Pattern Analysis and Machine Intelligence*, 35(8):1798–1828, 2013. 2
- [4] G. Chen, Y. Li, and S. N. Srihari. Word recognition with deep conditional random fields. In *IEEE Int. Conference on Image Processing (ICIP)*, pages 1928–1932, 2016. 2
- [5] A. Choromanska, M. Henaff, M. Mathieu, G. B. Arous, and Y. LeCun. The loss surfaces of multilayer networks. In *AISTATS*, 2015. 3
- [6] W. Chu and D. Cai. Deep feature based contextual model for object detection. *arXiv preprint arXiv:1604.04048*, 2016. 2, 6, 7
- [7] S. K. Divvala, D. Hoiem, J. H. Hays, A. A. Efros, and M. Hebert. An empirical study of context in object detection. In *IEEE Conf. on Computer Vision and Pattern Recognition*, pages 1271–1278, 2009. 2
- [8] T. Do and T. Arti. Neural conditional random fields. In *AISTATS*, 2010. 2
- [9] P. F. Felzenszwalb, R. B. Girshick, D. McAllester, and D. Ramanan. Object detection with discriminatively trained part-based models. *IEEE transactions on pattern analysis and machine intelligence*, 32(9):1627–1645, 2010. 2
- [10] S. Gidaris and N. Komodakis. Locnet: Improving localization accuracy for object detection. In *Proceedings of the IEEE Conference on Computer Vision and Pattern Recognition*, pages 789–798, 2016. 1
- [11] S. Gould, R. Fulton, and D. Koller. Decomposing a scene into geometric and semantically consistent regions. In *IEEE Int. Conference on Computer Vision*, pages 1–8, 2009. 2
- [12] K. He, X. Zhang, S. Ren, and J. Sun. Deep residual learning for image recognition. In *Proceedings of the IEEE Conference on Computer Vision and Pattern Recognition*, pages 770–778, 2016. 1
- [13] S. Hochreiter and J. Schmidhuber. Long short-term memory. *Neural computation*, 9(8):1735–1780, 1997. 7
- [14] N. Hu, G. Englebienne, Z. Lou, and B. Kröse. Learning latent structure for activity recognition. In *IEEE Int. Conf. on Robotics and Automation (ICRA)*, pages 1048–1053, 2014. 2
- [15] S. Ioffe and C. Szegedy. Batch normalization: Accelerating deep network training by reducing internal covariate shift. In *International Conference on Machine Learning (ICML)*, 2015. 5
- [16] S. Kakade, Y. W. Teh, and S. Roweis. An alternate objective function for markovian fields. In *International Conference on Machine Learning (ICML)*, 2002. 3
- [17] F. Korzenowski and G. Widmer. A fully convolutional deep auditory model for musical chord recognition. In *IEEE Int. Workshop on Machine Learning for Signal Processing (MLSP)*, pages 1–6, 2016. 2, 7
- [18] A. Krizhevsky, I. Sutskever, and G. E. Hinton. Imagenet classification with deep convolutional neural networks. In *Advances in neural information processing systems*, pages 1097–1105, 2012. 1, 2, 5
- [19] J. Lafferty, A. McCallum, and F. Pereira. Conditional random fields: Probabilistic models for segmenting and labeling sequence data. In *ICML*, pages 282–289, 2001. 2, 3
- [20] D. Lin, X. Shen, C. Lu, and J. Jia. Deep lac: Deep localization, alignment and classification for fine-grained recognition. In *The IEEE Conference on Computer Vision and Pattern Recognition (CVPR)*, 2015. 1
- [21] W. Liu, D. Anguelov, D. Erhan, C. Szegedy, S. Reed, C.-Y. Fu, and A. C. Berg. SSD: Single shot multibox detector. In *European Conference on Computer Vision*, pages 21–37. Springer, 2016. 1
- [22] A. McCallum, D. Freitag, and F. C. Pereira. Maximum entropy markov models for information extraction and segmentation. In *ICML*, pages 591–598, 2000. 3
- [23] J. Peng, L. Bo, and J. Xu. Conditional neural fields. In *Advances in neural information processing systems*, 2009. 2
- [24] J. Redmon and A. Farhadi. Yolo9000: Better, faster, stronger. *arXiv preprint arXiv:1612.08242*, 2016. 1
- [25] S. Ren, K. He, R. Girshick, and J. Sun. Faster r-cnn: Towards real-time object detection with region proposal networks. In *Advances in neural information processing systems*, pages 91–99, 2015. 1, 2
- [26] M. Schuster and K. K. Paliwal. Bidirectional recurrent neural networks. *IEEE Transactions on Signal Processing*, 45(11):2673–2681, 1997. 7
- [27] H. Schutze and J. Pedersen. A vector model for syntagmatic and paradigmatic relatedness. In *Proc. of the 9th Annual Conference of the UW Centre for the New OED and Tex*, 1993. 8
- [28] A. G. Schwing and R. Urtasun. Fully connected deep structured networks. *arXiv preprint arXiv:1503.02351*, 2015. 2
- [29] C. Sutton and A. McCallum. An introduction to conditional random fields for relational learning. *Introduction to statistical relational learning*, pages 93–128, 2006. 5
- [30] A. Torralba. Contextual priming for object detection. *International journal of computer vision*, 53(2):169–191, 2003. 2
- [31] Y. Wang and D. Wang. Cocktail party processing via structured prediction. In *Advances in Neural Information Processing Systems*, pages 224–232, 2012. 2
- [32] J. Yao, S. Fidler, and R. Urtasun. Describing the scene as a whole: Joint object detection, scene classification and semantic segmentation. In *IEEE Conf. on Computer Vision and Pattern Recognition (CVPR)*, pages 702–709, 2012. 2
- [33] N. Zhang, J. Donahue, R. Girshick, , and T. Darrell. Part-based r-cnns for fine-grained category detection. In *ECCV*. 1
- [34] S. Zheng, S. Jayasumana, B. Romera-Paredes, V. Vineet, Z. Su, D. Du, C. Huang, and P. H. Torr. Conditional random fields as recurrent neural networks. In *Proceedings of the IEEE International Conference on Computer Vision*, pages 1529–1537, 2015. 2